Molecular Crystals and Liquid Crystals
Publication details, including instructions for authors and subscription information:
http://www.tandfonline.com/loi/gmcl20

Effect of Zr Addition on Sol-Gel Processed InZrZnO Thin-Film Transistor

Dae-Hwan Kim [a], Dae-Ho Son [a], Shi-Joon Sung [a], Jung-Hye Kim [a] & Jin-Kyu Kang [a]

[a] Daegu Gyeongbuk Institute of Science and Technology (DGIST), 50-1 Sang-ri, Hyeonpung-myeon, Dalseong-gun, Daegu, 711-873, Republic of Korea

Version of record first published: 20 Aug 2012.

To cite this article: Dae-Hwan Kim , Dae-Ho Son , Shi-Joon Sung , Jung-Hye Kim & Jin-Kyu Kang (2012): Effect of Zr Addition on Sol-Gel Processed InZrZnO Thin-Film Transistor, Molecular Crystals and Liquid Crystals, 564:1, 130-137

To link to this article: http://dx.doi.org/10.1080/15421406.2012.691705

Mol. Cryst. Liq. Cryst., Vol. 564: pp. 130–137, 2012

ISSN: 1542-1406 print/1563-5287 online
DOI: 10.1080/15421406.2012.691705

Taylor & Francis
Taylor & Francis Group

Effect of Zr Addition on Sol-Gel Processed InZrZnO Thin-Film Transistor

DAE-HWAN KIM,* DAE-HO SON, SHI-JOON SUNG, JUNG-HYE KIM, AND JIN-KYU KANG

Daegu Gyeongbuk Institute of Science and Technology (DGIST), 50-1 Sang-ri, Hyeonpung-myeon, Dalseong-gun, Daegu 711-873, Republic of Korea

In this study, solution-processed InZrZnO thin films and a newly developed thin-film transistors (TFTs) were fabricated and characterized electrically. The InZrZnO TFTs were investigated according to the variation of the Zr-metal doping concentration. It was found that the off currents of InZrZnO TFTs were greatly influenced by the composition of Zr atoms suppressing formation of oxygen vacancies. The optimal transistor of InZrZnO channel layer shows good performance properties. The electrical characteristics of a 2.92 mol% Zr-doped InZnO TFT shows a field effect mobility of 0.05 $cm^2\ V^{-1}\ s^{-1}$, a threshold voltage of 6.1 V, an on/off ratio of 1.4×10^7, and a subthreshold swing of 0.42 V/dec. The InZrZnO TFT also shows better bias stability than undoped InZnO TFT, suggesting Zr plays a key role in regards to stability of TFT.

Keywords Metal oxide; thin film transistor; sol-gel; inzrzno; solution process; AMOLED

Introduction

In recent times, ZnO-based thin films have attracted considerable attention because of their numerous advantageous electrical and optical properties such as high mobility, high stability, and transparency [1,2]. For example, the use of ZnO, InZnO, ZnSnO, InGaZnO, and InZrZnO as active channel materials in thin-film transistors (TFTs) has been reported [3–6]. Such thin films have been deposited by vacuum deposition methods such as pulsed laser deposition (PLD), radio frequency (RF) or DC sputtering, and chemical vapor deposition. Although these methods are effective and highly reliable, they require expensive equipment, resulting in high manufacturing costs.

A simple and low-cost alternative to fabrication by vacuum deposition is solution-processed thin-film deposition, and several research efforts have been made in this direction. Recently, several papers have reported solution-based TFTs fabricated with ZnO, InZnO, MgZnO, ZnZrO, and InGaZnO [7–11]. These reports have attracted considerable attention because of the good electrical performance of the fabricated TFTs. In this study, we have newly developed solution-processed TFTs based on InZrZnO, a Zr-related multi-component transparent oxide, as the active layer. To the best of our knowledge, solution-processed

*Address correspondence to Dae-Hwan Kim, Green Energy Research Division, 50-1 Sang-ri, Hyeonpung-myeon, Dalseong-gun, Daegu 711-873, Republic of Korea. Tel: (+82)53-785-3720; Fax: (+82)53-785-3739. E-mail: monolith@dgist.ac.kr

InZrZnO transistors have not been fabricated thus far. We investigated the influence of the relative compositions of Zr on the electrical properties of TFTs to improve the on/off current level. We also investigated the influence of the relative compositions of Zr on the electrical properties of TFTs, such as on/off ratio, a field effect mobility and device stability.

Experimental

InZrZnO sol-gel solutions were prepared in the following manner. A mixture of indium nitrate hydrate ($In(NO_3)_3xH_2O$) and zinc acetate ($Zn(CH_3COO)_2$) was dissolved in acetyl acetone. The molar concentration of indium nitrate hydrate was 0.3 M (mole/liter) and that of zinc acetate was 0.1 M (mole/liter). Zirconium tert-butoxide ($Zr[OC(CH_3)_3]_4$) was added to the In-Zn solution with different Zr metal doping concentrations (0, 2.92, and 4.32 mol%). Then, monoethanolamine (MEA) and acetic acid (CH_3COOH) were added as sol stabilizers, and the resulting solution was stirred for 12 h. Thermally oxidized silicon substrates were used for fabricating spin-coated InZrZnO thin films. The silicon substrates were heavily doped with boron (p^+) to fabricate InZrZnO TFTs having an inverted-gate structure. After the SiO_2/Si substrate was cleaned, it was spin-coated with InZrZnO precursor solution at a speed of 5000 rpm for 30 s in a glove box. Then, the spin-coated substrate was oxidized in a tube furnace at 500°C for 1 h in an oxygen ambient atmosphere with a flow rate of 200 sccm. Further, 100-nm-thick Al source and drain contacts were vapor deposited on the active layer of the substrate through a shadow mask. The length and width of the channel were 40 μm and 1000 μm, respectively. The electrical characteristics of the InZrZnO TFTs were measured using a Keithley 4200-SCS semiconductor parameter analyzer. The microstructure and surface morphology were also observed by scanning electron microscope (SEM) and atomic-force microscope (AFM).

Results and Discussion

Figure 1 (a) shows the schematic cross section of the InZrZnO TFT having an inverted-staggered bottom-gate structure. Figure 1 (b) shows the cross-sectional SEM image of the InZrZnO (2.92 mol% Zr-doped InZnO TFT) thin film fabricated on an approximately 30-nm-thick SiO_2/Si substrate. Figure 2 shows the SEM plan-view and AFM image of InZrZnO thin films with different Zr metal doping concentrations. Irrespective of the Zr doping concentration, the Zr-doped samples exhibited a very uniform and smooth morphology with a thickness of around 30 nm in SEM plan view image. In addition, the surface roughness of the Zr-doped InZnO (4.32 mol% Zr-doped InZnO; $R_{rms} = 1.347$ nm) was greater than pure InZnO (0 mol% Zr-doped InZnO; $R_{rms} = 0.147$ nm) measured by AFM. We also observed that the surface roughness of the thin film appeared to be increased by the addition of Zr. However, surface roughness of the Zr-doped InZnO films has sufficiently low value in the range of 0.147 nm$\sim$1.347 nm, which indicates InZrZnO TFTs fabricated by the sol-gel method can be used as an active channel layer.

X-ray photoelectron spectroscopy (XPS) measurements were performed to determine the relative quantitative chemical properties of InZrZnO thin films and obtain their binding information. After the carbon contamination of InZrZnO thin film was removed by Ar^+ sputtering, XPS analysis was carried out to quantitatively establish the chemical properties of the InZrZnO thin films. And all the spectra are calibrated by setting the C1s peak at 284.6 eV. Table 1 summarizes the atomic concentration of the InZrZnO films, as determined by XPS. The atomic concentration was determined by normalizing the integrated photoemission intensity of each element to its atomic sensitivity factors. Figure 3 shows

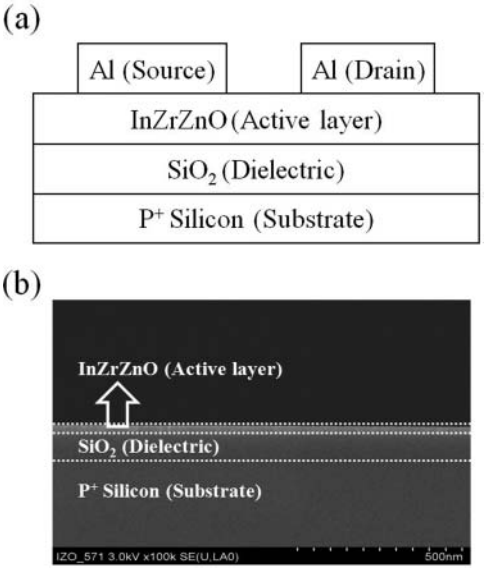

Figure 1. (a) Schematic structure of InZnZrO TFT and (b) cross-sectional SEM image of 2.92 mol% Zr-doped InZnO thin film.

(a) In 3d, (b) Zr 3d, (c) Zn 2p, and (d) O 1s of the XPS spectra of InZrZnO (2.92 mol% Zr-doped InZnO) thin films. In this figure, the observed binding energy peaks located at (a) 444.0, (b) 181.2, and (c) 1020.9 eV correspond to In-O, Zr-O, and Zn-O bonds, respectively. The O 1s peak splits into two components located at 529.2 eV and 530.4 eV. The low binding energy is attributed to O^{2-} ions surrounded by In, Zr, and Zn atoms in InZrZnO matrix system. The high binding energy component can be associated with O^{2-} ions that exist in oxygen deficient regions in InZrZnO matrix system. Thus, the change in the intensity of this peak can be related to the variation in the concentration of oxygen vacancies. Figure 4 shows the O 1s (a) and Zr 3d (b) core-level XPS spectra at the indicated Zr metal doping concentrations. In the 4.32 mol% Zr-doped InZnO thin film, the O 1s core-level spectrum shifted to a lower binding energy level by 1.6 eV compared to that of the 0 mol% Zr-doped InZnO thin film as shown in Fig. 4(a). The downward shift of binding energy can be related to the decrease of oxygen vacancies in InZrZnO thin film. In addition, the obvious increase of Zr 3d peak, that leads to the decrease in oxygen vacancy, with the increase of Zr doping concentration is shown in Fig. 4(b). From the results of O1s peak fitting, it was found that the normalized portion of metal-oxygen bond in O 1s peak are 62% and 88% for 0 mol% and 4.32% Zr-doped InZnO thin film respectively as shown in Fig. 4(a). The increased portion of metal-oxygen bond component in 4.32%

Table 1. Atomic concentration of InZrZnO thin film determined by XPS

Zr mol%	In 3d	Zr 3d	Zn 2p	O 1s
0%	38.66	—	10.01	51.33
2.92%	39.77	2.41	6.79	51.03
4.32%	32.83	3.68	9.54	53.95

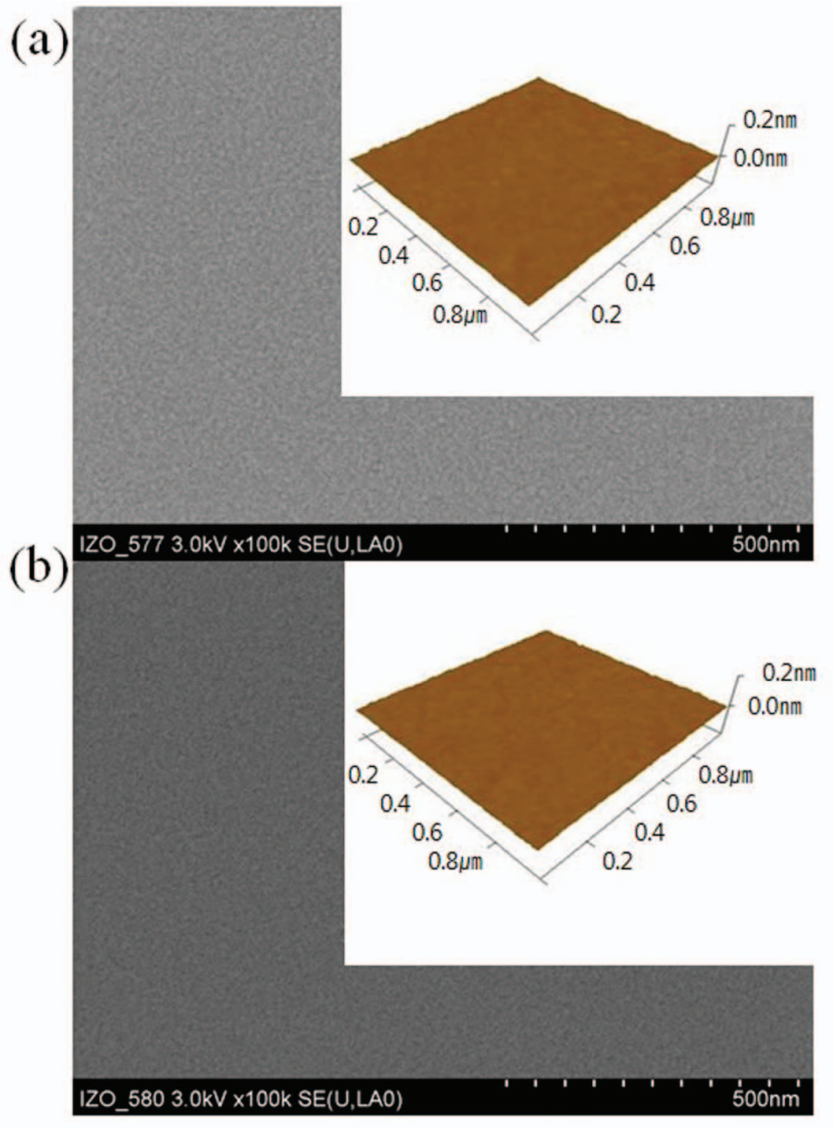

Figure 2. SEM plan-view and AFM image (inset) of InZrZnO thin film: 0 (a) and 4.32 (b) mol% Zr-doped InZnO.

Zr-doped InZnO thin film is obviously in connection with the decrease of oxygen vacancies. To confirm a relationship between Zr and free carrier electrons, capacitance-voltage characteristics of metal-insulator-semiconductor structures with different Zr metal doping concentrations were measured, as shown in the inset of Fig. 4(c). The carrier concentration was extracted by $n = 2/[q\varepsilon_s A^2(dC^{-2}/dV)]$, where q is the electron charge, k is dielectric constant, ε_s is the permittivity of the InZrZnO and A is electrode area [10,12]. The carrier concentration, as shown in Fig. 4(c), was decreased from 1.05×10^{16} to 4.66×10^{15} with the increase in the Zr-doped ratio from 0 to 4.32, respectively, which accords closely with above XPS analysis.

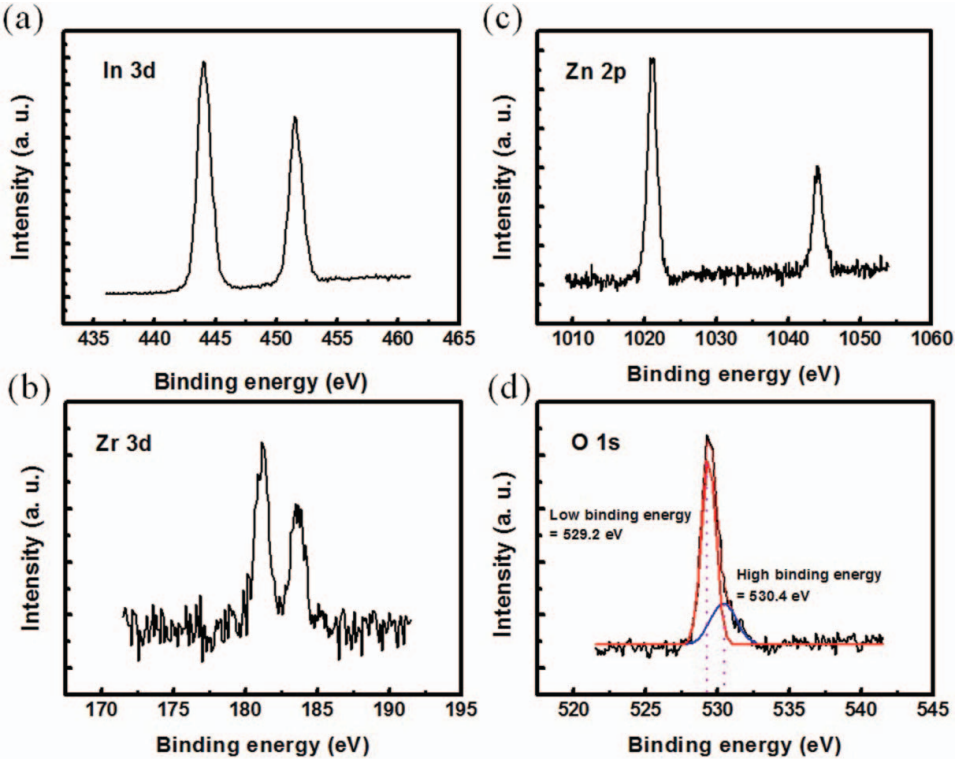

Figure 3. (a) In 3d, (b) Zr 3d, (c) Zn 2p, and (d) O 1s core-level XPS spectra of 2.92 mol% Zr-doped InZnO thin film.

Figure 5 (a) shows the drain current-gate voltage (I_{DS}-V_{GS}) characteristics of InZr ZnO TFTs with various concentrations of Zr at $V_{DS} = 20$ V. The operating voltage of InZrZnO TFTs was lower than one of the ZnZrO TFTs described [10]. When the Zr doping ratio increases, the off current and the field-effect mobility in the transfer curve of InZrZnO TFTs decrease. Although the drain current (I_{ON}) decreased slightly with an increase in the Zr doping ratio, the I_{on}/I_{OFF} current ratio increased considerably, and the threshold voltage was shifted to a positive voltage direction. These results indicate that the carrier concentration in the active channel layer of InZrZnO changed with the Zr doping ratio. This XPS results and TFT properties clearly show the important role of Zr material in the InZrZnO thin film. Further, because the Zr ions (Zr = 1.33) in InZrZnO thin films are highly electronegative, they form stronger chemical bonds than In and Zn ions with O, and hence, they play a more important role in the electrical characteristics of the thin films [6]. In addition, the suppressing the formation of free carrier or oxygen vacancy for Zr ions is similar to those reported for other material such as Ga and Hf [13,14]. Figure 5 (b) and (c) show the performance of an InZrZnO (2.92 mol% Zr-doped InZnO) TFT with a channel width and channel length of 1000 μm and 40 μm, respectively. The electrical parameters including the saturation field effect mobility and threshold voltage were derived by linear fitting to the plot of the square root of the drain current versus the gate voltage. The following equation is the general expression for the operation of a field-effect transistor

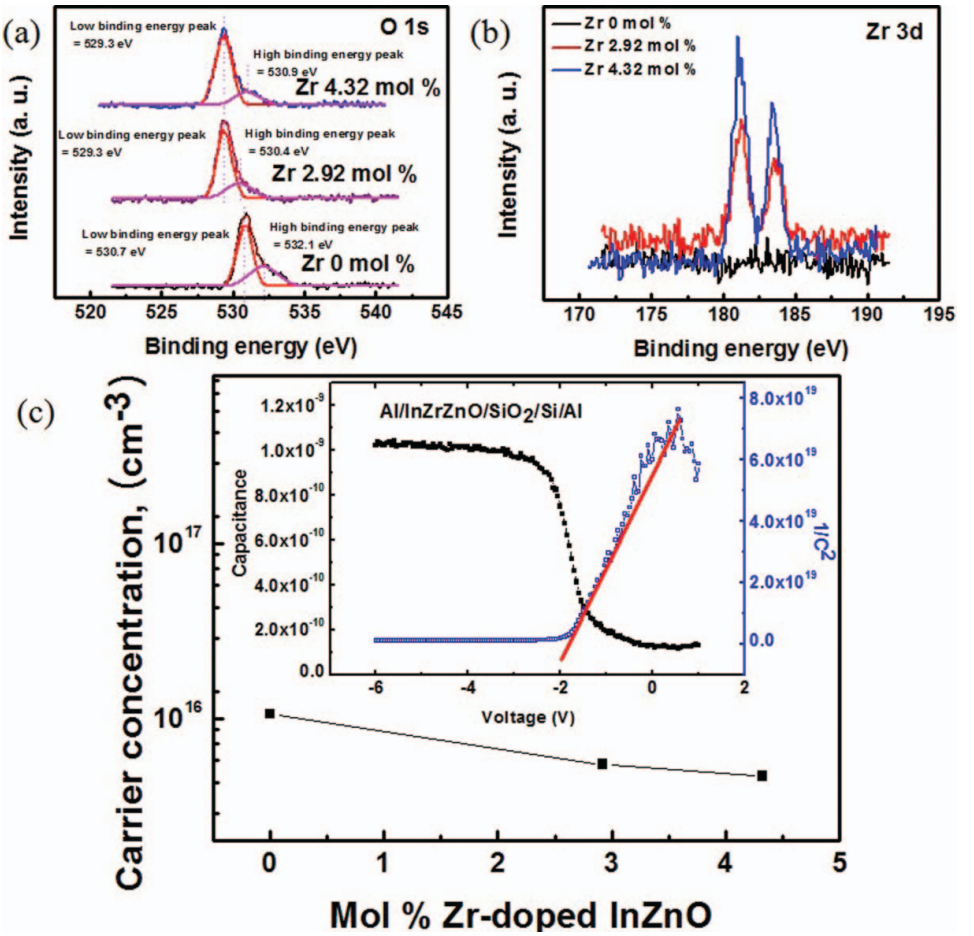

Figure 4. (a) O 1s and (b) Zr 3d core-level XPS spectra at the indicated mol% Zr-doped InZnO. (c) Carrier concentration in the InZrZnO films with different Zr-doped. Inset shows the plot of C-V and $1/C^2$-V curves of MOS structure (Al/2.92 mol% Zr-doped InZnO/SiO_2/Si/Al).

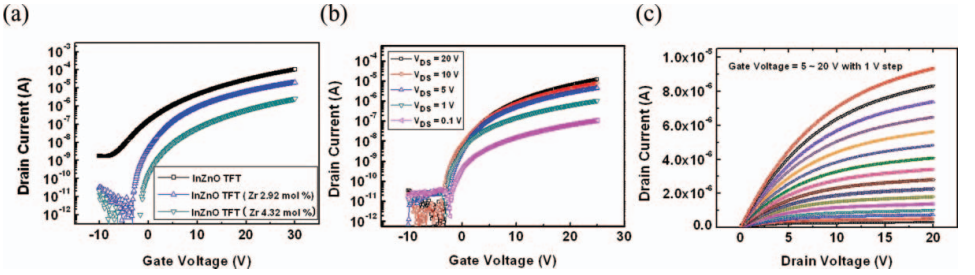

Figure 5. (a) Transfer characteristics of InZrZnO TFTs for different values of Zr, (b) transfer and (c) output characteristics of 2.92 mol% Zr-doped InZnO TFTs annealed at 500°C for 1 h.

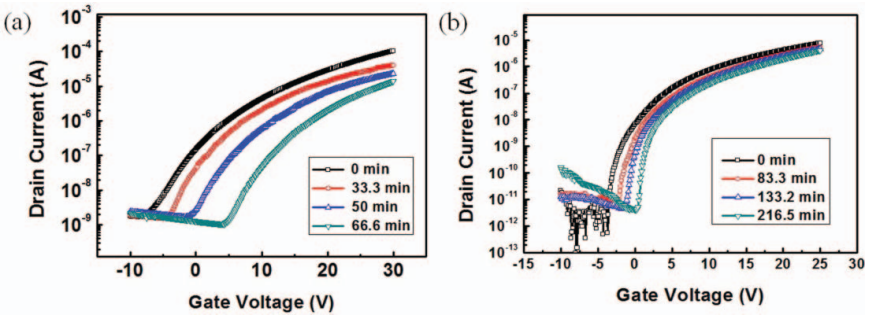

Figure 6. (a) Transfer curve shifts of non-passivated InZnO TFT and (b) InZrZnO TFTs under drain current stress of 1 μA at $V_{DS} = 10$ V for the indicated time in 60% ambient relative humidity.

in the saturation region [12]

$$I_{DS} = \left(\frac{WC_i\mu_{sat}}{2L}\right)(V_{GS} - V_{th})^2 \text{ for } V_{DS} > V_{GS} - V_{th}$$

where W is the channel width; L, the channel length; C_i, the capacitance per unit area of the gate insulator; V_G, the gate voltage; I_D, the drain to source current; and V_{th}, the threshold voltage of the TFT. As shown in Fig. 5(a), the electrical performance of the 2.92 mol% Zr-doped TFT was the best among the three different transistors. From Eq. (1), it was found that the 2.92 mol% Zr-doped InZrZnO TFT exhibited a subthreshold slope (S.S) of 0.42 V/dec, I_{ON}/I_{OFF} of 2.2×10 [7], threshold voltage of 6.1 V, and saturation field effect mobility of 0.05 $cm^2\ V^{-1}\ s^{-1}$. In addition, it also exhibited an expected gate modulation of drain current (I_{DS}) in both the linear and the saturation regimes. Finally, to examine the effect of Zr material on the device stability, the V_{th} shifts of the two different transistors under constant current bias stress were measured. Fig. 6 shows the variations of the transfer characteristics of the non-passivated 2.92 mol% Zr-doped InZrZnO TFT and non-passivated InZnO TFT under drain current stress of 1 μA at $V_{DS} = 10$ V for the indicated time in 60% ambient relative humidity. The InZnO TFT showed a large positive voltage shift of about 13 V in V_{th} after applying drain current stress of 66.6 minutes, on the other hand, the Zr-doped InZrZnO TFT showed a small positive shift of about 4 V in V_{th} even after 216.5 minutes. In our experiments, even though InZnO and InZrZnO TFT have identical gate insulator and device structure, the significantly different V_{th} shift behaviors appeared during the drain current stress. The enhanced stability of the InZrZnO TFT device can be attributed to the presence of Zr material in the active channel layer. Since Zr has high oxygen bonding energy, it can play a key role in improving of TFT stability. This result agrees well with recent reports of oxide transistors having high k materials [6,15].

Conclusions

This letter describes a newly developed TFT with a synthesized multi-component material InZrZnO channel layer. Thin films of InZrZnO TFTs were formed by the sol-gel method. The results show that the critical Zr doping concentration improves the electrical properties of TFTs. The off current of InZrZnO TFT was suppressed due to the variation of carrier concentration in active channel layers with more Zr-metal doping concentration. The optimal transistor of InZrZnO channel layer exhibited the high performance properties. The

device fabricated with the 2.92 mol% Zr-doped InZnO thin film yielded S.S 0.42 V/dec, I_{ON}/I_{OFF} of 2.2×10^7, threshold voltage of 6.1 V, and saturation field effect mobility of 0.05 $cm^2\ V^{-1}\ s^{-1}$. We also investigated the stability of TFTs at same drain current stress. Two active layer types of TFTs, one having an InZnO and the other having an InZrZnO channel layer, were compared. The latter exhibits better stability, indicating a significant role of Zr material in device stability. These results demonstrate that the simple solution process of InZrZnO channel layer can possibly be used for the fabrication of display driving devices.

Acknowledgment

This work was supported by DGIST R&D Program of the Ministry of Education Science and Technology of Korea (11-BD-05). We thank Dr. Bae of the Korea Basic Science Institute in Busan center for obtaining the XPS spectra.

References

[1] Carcia, P. F., McLean, R. S., Reilly, M. H., & Nunes, G., Jr. (2003). *Appl. Phys. Lett.*, *82*, 1117.
[2] Nomura, K., Ohta, H., Ueda, K., Kamiya, T., Hirano, M., & Hosono, H. (2003). *Science*, *300*, 1269.
[3] Wang, Y. L., Ren, F., Lim, W., Norton, D. P., Pearton, S. J., Kravchenko, I. I., & Zavada, J. M. (2007). *Appl. Phys. Lett.*, *90*, 232103.
[4] Chiang, H. Q., Wager, J. F., Hoffman, R. L., Jeong, J., & Keszler, D. A. (2005). *Appl. Phys. Lett.*, *86*, 013503.
[5] Nomura, K., Ohta, H., Takagi, A., Kamiya, T., Hirano, M., & Hosono, H. (2004). *Nature*, *432*, 488.
[6] Park, J. S., Kim, K. S., Park, Y. G., Mo, Y. G., Kim, H. D., & Jeong, J. K. (2009). *Adv. Mater.*, *21*, 329.
[7] Ohya, Y., Niwa, T., Ban, T., & Takahashi, Y. (2001). *Jpn, J. Appl. Phys.*, *40*, 297.
[8] Lee, D. H., Chang, Y. J., Herman, G. S., & Chang, C. H. (2007). *Adv. Mater.*, *19*, 843.
[9] Tsay, C. Y., Cheng, H. C., Wang, M. C., Lee, P. Y., Chen, C. F., & Lin, C. K. (2007). *Surf. Coat. Technol.*, *202*, 1323.
[10] Lee, J. H., Lin, P., Ho, J. C., & Lee, C. C. (2006). *Electrochem. Solid-State Lett.*, *9*, G117.
[11] Kim, G. H., Ahn, B. D., Shin, H. S., Jeong, W. H., Kim, H. J., & Kim, H. J. (2009). *Appl. Phys. Lett.*, *94*, 233501.
[12] Schroder, D. K. (2006). *Semiconductor Material and Device Characterization,* 3rd ed. Wiley, New York.
[13] Hosono, H. (2006). *J. Non-Cryst. Solids.*, *352*, 851.
[14] Son, D. H., Kim, D. H., Kim, J. H., Sung, S. J., Jung, E. A., & Kamg, J. K. (2010). *Electrochem. Solid-State Lett.*, *13*, H274.
[15] Kim, C. J., Kim, S., Lee, J. H., Park, J. S., Kim, S., Park, J., Lee, E., Lee, J. C., Park, Y. S., Kim, J. H., Shin, S. T., & Chung, U. I. (2009). *Appl. Phys. Lett.*, *95*, 252103.